

# Wake analysis of drag components in gliding flight of a jackdaw (*Corvus monedula*) during moult

Marco KleinHeerenbrink and Anders Hedenström\*

Dept. of Biology, Lund University, Sölvegatan 37, SE-223 62 Lund, Sweden

Author Accepted Manuscript

Accepted for publication 8th November 2016

Publisher version: KleinHeerenbrink, Hedenström A. 2017 Wake analysis of drag components in gliding flight of a jackdaw (*Corvus monedula*) during moult. *Interface Focus* 20160081. (doi:10.1098/rsfs.2016.0081)

## Abstract

To maintain the quality of the feathers, birds regularly undergo moult. It is widely accepted that moult affects flight performance, but the specific aerodynamic consequences have received relatively little attention. Here we measured the components of aerodynamic drag from the wake behind a gliding jackdaw (*Corvus monedula*) at different stages of its natural wing moult. We found that span efficiency was reduced (lift induced drag increased) and the wing profile drag coefficient was increased. Both effects best correlated with the corresponding reduction in spanwise camber. The negative effects are partially mitigated by adjustments of wing posture to minimize gaps in the wing, and by weight loss to reduce wing loading. By studying the aerodynamic consequences of moult we can refine our understanding of the emergence of various moulting strategies found among birds.

## 1. Introduction

Over time the quality of the feathers deteriorates, so birds regularly undergo moult to replace old, worn, feathers. The loss of flight feathers poses a potential challenge to birds with respect to flight performance, due to the reduced wing area and altered wing shape due to missing feathers [1, 2]. Some species lose all flight feathers simultaneously, which renders them flightless for some time [e.g. 3, 4]. Other birds are highly dependent on their flight capacities (e.g. large birds of prey, swifts and many seabirds), so they spread their moult over several months [5] or even years [6–11]. Most passerines have an annual moult of flight feathers, generally taking place in the time between breeding season and autumn migration. Pressured by time, they face a compromise between duration of the moult and the performance reduction related to moult gaps [12]. In some long-distance migrants moult tends to take place after the completion of autumn migration [13].

Even though it is widely accepted that moult affects flight performance, the aerodynamic consequences

have so far received little attention. Tucker [14] measured the variation in the maximum glide performance curve, i.e. the lift to drag ratio, for a Harris' hawk (*Parabuteo unicinctus*) that went through a natural moult cycle. He found that the maximum lift to drag dropped from 10.5 to a worst case of about 7 at peak primary moult. Chai [15] studied hovering performance of hummingbirds (*Archilochus colubris*), both during natural moult and by wing manipulations and found that hummingbirds were still able to fly with a 30% decrease in wing area, compensating by reducing their body mass. Several studies, e.g. Lind [16] and Williams & Swaddle [17], measured reduced escape performance in moulting birds. In a study on the wake of blackcaps (*Sylvia atricapella* L.) Johansson & Hedenström [18] described an accidental fright moult of the tail, but found this had no noticeable effects on the thrust production in forward flight.

With the current study we aim to shed light on the underlying aerodynamic consequences of moult. We measured the components of aerodynamic drag from the wake behind a gliding jackdaw (*Corvus monedula*) at different stages of its natural wing moult. In glid-

ing flight weight is balanced by the aerodynamic forces acting on the wing and body of the bird. By definition we can decompose the resultant aerodynamic force into lift  $L = W \cos \gamma$  (perpendicular to the flight path) and drag  $D = W \sin \gamma$  (along the flight path), where  $\gamma$  is the angle between the flight path and the horizontal plane. Drag can be decomposed into three major components:  $D = D_{\text{ind}} + D_{\text{pro}} + D_{\text{par}}$ .

Induced drag is the cost of lift production:

$$D_{\text{ind}} = \frac{L^2}{q\pi eb_w^2}, \quad (1)$$

where  $q = \frac{1}{2}\rho U_\infty^2$ ,  $\rho$  is the air density,  $U_\infty$  is the air speed, and  $e$  is the span efficiency factor indicating how effective the available wingspan ( $b_w$ ) is used for producing lift. In steady gliding flight, the bird can adjust its wingspan [19], and it may have limited control over the efficiency of the wing [20, 21]. We hypothesise that moult gaps will affect these two variables. Wingspan can be affected either by direct reduction of the maximum wingspan during moult of the outer primaries, or by the bird partially folding the wing to reduce gaps along the trailing edge of the wing. Span efficiency may be affected by changes in lift distribution [2], or by reducing the vertical separation of the outer primary feathers [22].

Profile drag represents the more localized interaction between the wing surface and the flow:

$$D_{\text{pro}} = qC_{D,\text{pro}}S_w. \quad (2)$$

Here  $S_w$  is the projected area of the wing and  $C_{D,\text{pro}}$  is a coefficient representing a characteristic property of the wing profile. When a bird flexes its wings the wing area varies approximately linearly with the wingspan, and the accompanying reduction in profile drag is thought to be the reason why birds flex their wings at higher flight speeds [19]. For most aerofoils the profile drag coefficient  $C_{D,\text{pro}}$  is a quadratic function of lift coefficient:  $C_{D,\text{pro}} = C_{D,\text{pro},\text{min}} + k_p (C_L - C_{L D_{\text{pro},\text{min}}})^2$ , where  $C_L = L/qS_w$ . Here,  $C_{D,\text{pro},\text{min}}$  is the minimum profile drag coefficient corresponding to the lift coefficient  $C_{L D_{\text{pro},\text{min}}}$ . The factor  $k_p$  determines the degree of the lift dependency. The  $C'_{D,\text{pro},\text{min}}$ ,  $C_{L D_{\text{pro},\text{min}}}$  and  $k_p$  are characteristic for the specific wing shape. As the moult affects the wing shape, we expect these coefficients to vary throughout the process.

Finally, parasitic drag is associated with moving the body, and any appendages besides the wings, through the flow. We will refer to this component as body drag,

as the body is the most contributor to this drag. It can be expressed as

$$D_{\text{par}} = qC_{D,\text{par}}S_b, \quad (3)$$

where  $S_b$  represents the body frontal area and  $C_{D,\text{par}}$  is the body drag coefficient. Body frontal area is presumably unaffected by wing moult. However, the drag on the tail is inseparable from that of the body, so that moult of tail feathers could affect the body drag directly. The tail is also used to balance the aerodynamic forces around the centre of mass [23]. We expect that the moult will alter the lift distribution on the wings so that we will observe a change in the body drag coefficient.

## 2. Materials and methods

### 2.1. Experimental setup

For the experiments we used the low-turbulence tiltable wind tunnel at the Department of Biology, Lund University, Sweden [24]. The octagonal test section is 1.20 m wide, 1.08 m high and the closed section is approximately 1.2 m long. Downstream of this section is an approximately 0.5 m long gap that allows easy access to the bird.

The velocity field in a plane perpendicular to the free stream flow in the wake behind the bird was measured using a Particle Image Velocimetry (PIV) system recording 640 frame-pairs per second. Two LaVision Imager pro HS 4M (LaVision GmbH, Goettingen, Germany) high speed cameras 2016x2016 px in stereo configuration were aimed at the left wing tip vortex and an additional two cameras were aimed at the inner wing and body wake region. The combined resolved flow field had a width of 0.45 m and a height of 0.35 m. A 527 nm diode pumped LDY304PIV laser (Litron Lasers Ltd, Rugby, England) was used to illuminate particles ( $\sim 1 \mu\text{m}$ ) in a sheet, approximately 3 mm thick in the streamwise direction, aligned with the plane of focus of the cameras (figure 1).

The posture of the bird was captured using two LaVision HighSpeedStar3 high speed cameras  $1024 \times 1024$  px in dorsal view stereo configuration (figure 1). The cameras were calibrated with a moving checkerboard pattern using routines from the Matlab Computer Vision Toolbox (The Mathworks Inc, Natick, MA, USA).

### 2.2. Study species

A young jackdaw was taken from a study colony near Revingehed, Skåne, Sweden, around the time of fledging (June 11, 2013). The bird was kept in an

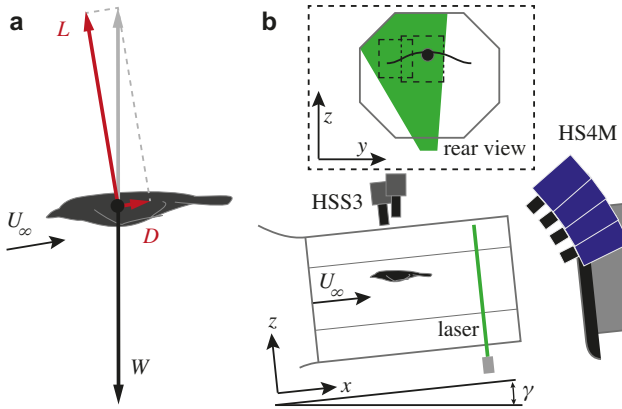


**Figure 1:** (a) Force balance on a bird in steady glide. The vector sum of lift  $L$  and drag  $D$  balance the weight  $W$ . (b) The wind tunnel is tilted to a glide angle  $\gamma = 6.0^\circ$ . Two high-speed cameras (HSS3) record the posture of the gliding bird. Four high-speed cameras (HS4M) record the movement of suspended oil droplets, which are illuminated by a laser sheet (laser). The inset (rear view) shows the two fields of view of the double stereo PIV configuration: one capturing the wake from the wing tip and the other capturing the wake from the central wing and body.

indoor aviary measuring  $1.5 \text{ m} \times 1.5 \text{ m} \times 2 \text{ m}$ . Food and water were made available ad libitum. Food and bathing water were removed one hour before training or experiments, to keep the bird motivated and to prevent it from getting soaked. The bird was trained, using positive reinforcement (audible cues followed by a food reward), to return to the experimenter's hand, to stand on a digital weighing balance, and to keep position when flying in the wind tunnel. (The bird was first used in experiments reported elsewhere [25]). Following Pennycuik [26], maximum wingspan was measured from the bird in the hand, being  $b_w = 0.67 \text{ m}$  and wing area was determined from a tracing of the left wing:  $S_w = 0.0652 \text{ m}^2$  (including both wings and the area between the wing roots). For body frontal area we used the relation  $S_b = 0.0129 m_B^{0.614}$  from Hedenström & Rosén [27], which was based on a wide range of passerines, including two jackdaws. Body mass ( $m_B$ ) was measured daily and was typically  $0.215 \text{ kg}$ , resulting in a body frontal area  $S_b = 0.00502 \text{ m}^2$ .

### 2.3. Posture reconstruction

In each view several key points were digitized as shown in figure 2; the tip of the primary feathers (1-10), the tip of the secondary feathers (11-18), tertials (19-20), tip of the rectrices (21-26), body centre line (27-28), the shoulder (29) and the wrist (30). Points 19, 20 and 27 to 30 are not physical marks consistent over all sequences. Instead marks were identified within each se-

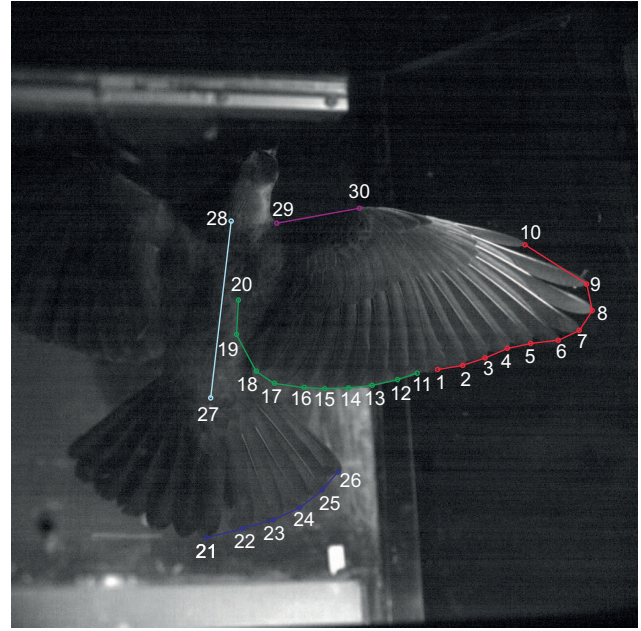


**Figure 2:** Posture analysis. Primary feathers: red line points 1 to 10 (outwards); Secondary feathers and tertials: green line points 11 to 20 (inwards); Rectrices: blue line points 21 to 26 (outwards); Body centre points: cyan line points 27 to 28; Shoulder (29) to wrist (30) purple line.

quence. Point 28 (neck) is located at the collar at the transition between fine feathers on the head and the larger body feathers. The feathers on the head meet at the centre line of the head, resulting in temporary natural markers that could be identified in both views throughout several frames. Point 27 (rump) is horizontally aligned between the two central rectrices. The streamwise location is determined similarly to point 28.

The reconstructed points were mirrored in the sagittal plane (through points 27-28), and the result was visually checked for errors. Inflight wingspan ( $b'_w$ ) was determined from the maximum distances between any primary feather point to its respective mirrored point. We define span ratio as the ratio between inflight span and maximum wingspan:  $\beta = b'_w/b_w$ . Wing area ( $S'_w$ ) was computed as the area enclosed between points 1 to 18, 29, 30, and their mirrored points (excluding missing feathers). This means the wing root is taken as the line between the shoulder and the tip of T8. We define wing area ratio as  $\zeta = S'_w/S_w$ .

Tail span ( $b'_t$  and  $\beta_t = b'_t/b_w$ ) was determined in the same way as wingspan by using the rectrix points instead. For the tail area ( $S'_t$ ) an additional point was required, which was positioned 1/3 the distance from the rump to neck (approximately extension of R6 to body centre line in figure 2). Body angle ( $\alpha_b$ ) was determined from the  $x$  and  $z$  coordinates of points 27 and 28.

To calculate the spanwise camber a polynomial

$$\hat{z} = c_0 + c_2\hat{y}^2 + c_4\hat{y}^4$$

was fitted through the trailing edge of the main wing (points 1-6 and 11-16), using the Matlab fit() function, to characterize the shape of the wing (here  $\hat{y} = y/b'_w$  and  $\hat{z} = z/b'_w$  are centred around the mean of all wing points). The spanwise camber (maximum height difference) was calculated as the vertical distance between the wing root and the lowest point of the trailing edge shape

$$\eta_w = c_0 - \hat{z}_{\min},$$

where  $\hat{z}_{\min}$  is the minimum value of  $\hat{z}$  on the domain  $-\frac{1}{2} \leq \hat{y} \leq \frac{1}{2}$ . This definition corresponds to the typical anhedral observed for the jackdaw. Vertical separation of the outer primaries ( $\eta_{p,i=7..10}$ ) was calculated as the vertical distance of the feather tip to the fitted trailing edge shape of the main wing. Tail separation  $\eta_t$  (the vertical gap between the main wing and tail trailing edge) was computed as the difference in mean height between the secondaries (11-18) and the rectrices (21-26), normalized by  $b'_w$ .

## 2.4. Wake analysis

The wake velocity fields were computed in LaVision Davis 8.1.5 using a weighted sliding sum of correlation routine (multipass with final size  $16 \times 16$  px; 50% overlap). This routine was chosen to compensate the low correlations due to particle loss (due to the largest particle displacement occurring in the smallest dimension of the laser sheet). The raw vector fields were further processed in Matlab. At each speed each view showed a small (within a range  $\pm 2\%$  of mean velocity) but distinct false pattern in the background flow in the streamwise direction, most likely due to the relatively high velocity perpendicular to the measurement plane. This pattern was removed by constructing an average second order surface polynomial that was subtracted from the measured flow, and replaced this with a uniform streamwise velocity based on the mean velocity from the polynomial. Then the two views were merged using weighted averaging, favouring vectors with low temporal signal noise. From the merged velocity field sequences, segments of 40 to 60 frames (63-94ms) were selected, during which the wake did not notably displace or change shape. For these segments the time average velocity field  $\bar{\mathbf{u}}$  and the root mean squared time fluctuations  $\mathbf{u}'$  were computed. As only the wake from the left wing and the body were captured, a symmetry-plane was defined manually, depending on the available information in the wake to

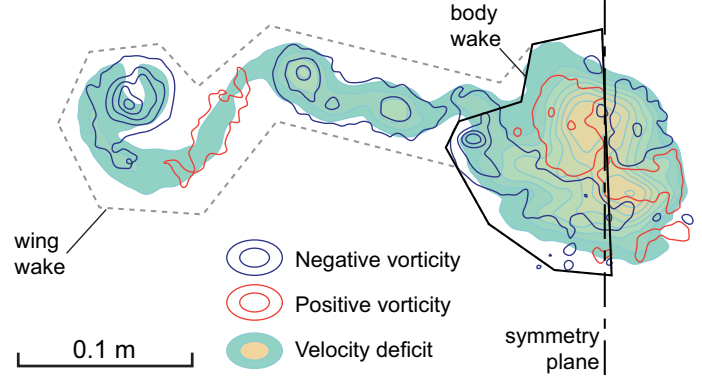


**Figure 3:** Wake regions of interest. Dashed line: region of interest containing all vorticity and streamwise perturbations. Black solid line: body drag region containing all streamwise perturbations attributed to body and tail (In this particular case only half the body wake was used, and multiplied by 2). Dash-dot vertical line: symmetry plane to mirror vorticity to the right. This specific case is of moult stage I at  $7.8 \text{ m s}^{-1}$ .

best estimate the location of the right wing tip vortex (see figure 3).

Lift was computed using

$$L = \rho \iint y \bar{w} dS + \rho \iint \rho y \left\{ \bar{w} \frac{\partial \bar{u}}{\partial y} - \bar{v} \frac{\partial \bar{u}}{\partial z} \right\} dS, \quad (4)$$

where  $\bar{w} = (\nabla \times \bar{\mathbf{u}}) \cdot \mathbf{i}$  (see e.g. van Dam *et al.* [28] for a derivation). Induced drag was computed as

$$D_{\text{ind}} = \frac{1}{2} \rho \iint \psi \bar{w} dS + \frac{1}{2} \rho \iint (v'^2 + w'^2) dS, \quad (5)$$

where  $\psi$  is the cross-flow streamfunction. The streamfunction is solved from  $\nabla^2 \psi = -\bar{w}$  with Dirichlet boundary conditions  $\psi = 0$  at the wind tunnel walls (using function `adaptmesh()` from the Matlab Partial Differential Equation toolbox (The Mathworks Inc, Natick, MA, USA)). Body drag was computed as

$$D_{\text{par}} = \rho \iint_{\text{body}} (\bar{u} (U_\infty - \bar{u})) dS - \rho \iint_{\text{body}} u'^2 dS, \quad (6)$$

where the body region was defined manually for every wake based on the pattern of the streamwise velocity perturbation (see figure 3). Profile drag of the tail is included in this body drag term, even when the tail was widely spread. Wing profile drag was computed using

$$D_{\text{pro}} = \rho \iint_{\text{pro}} (\bar{u} (U_\infty - \bar{u})) dS - \rho \iint_{\text{pro}} u'^2 dS, \quad (7)$$

where the profile drag region was defined manually to include only the velocity deficit due to the wing and to

minimize the influence of noise outside of the actual wake (see figure 3).

Equation 5 only takes into account the affected air-stream within the boundaries of the wind tunnel walls, which results in a reduction of induced drag compared to what the same distribution of vorticity would produce in an unbounded flow. Shape specific span efficiency  $e'$  was corrected for this wall effect by

$$e' = \left( \beta^2 / e + \sigma \right)^{-1}, \quad (8)$$

where we used the wall correction  $\sigma = 0.108 + 0.005(b'_w/B)$ , with  $B$  representing the width of the test section. We determined this correction numerically for this wind tunnel by computing the induced drag of a simulated vortex pair for different wind tunnel sizes. Effects of wake blockage and solid blockage were found to be negligible:  $(\Delta u/U_\infty)_{wb/sb} \ll 1\%$ ; Barlow *et al.* [29, p. 374].

## 2.5. Weight support

For perfect steady gliding flight the total aerodynamic force balances the weight of the bird. In that case the weight support  $(L^2 + D^2)^{1/2} / W = 1$ . We only used sequences where weight support, based on the wake measurements, was between 80% and 120%, which resulted in a dataset of 212 sequences with an average weight support of  $1.03 \pm 0.08$  (mean  $\pm$  s.d.).

## 2.6. Statistics

To test the effects of the moult stages on the measures of posture and the various aerodynamic parameters, we used the `fitlm()` function from the Matlab Statistics Toolbox (The Mathworks Inc, Natick, MA, USA), including the moult stage (MS) as a categorical variable and all other variables as continuous variables. In the following section we adopted the Wilkinson notation for describing the regression models ( $y \sim 1 + x_1 + x_2 * x_3$  representing  $y = \beta_0 + \beta_1 x_1 + \beta_2 x_2 + \beta_3 x_3 + \beta_{2,3} x_2 x_3$ ). For including higher order terms (e.g.  $y \sim U * U * MS$ ) we used the function `stepwiselm()`, removing higher order terms according to the default 'sse' criterion. Because stage I contained only few data points, it was excluded from the model selection step. For the regressions with profile drag, outliers were identified through robust bilinear weighting. Data points that were assigned zero weight were removed before refitting the model.

## 3. Results

### 3.1. Moulting process

The bird started moult of the flight feathers at the 15th of April 2014, loosing both inner primaries (P1) simultaneously, followed by shedding P2 two days later. P3, P4 and P5 were then shed at intervals of about one week. The remaining primary pairs were shed sequentially every other week (see figure 4), ending with P10 on the 30th of July. The moult of secondary feathers started from S1 at the 3rd and 4th of June (49 days after P1), progressing inwards at two week intervals until S5/S6. The right S6 was dropped one day after the right S5 and a day after both S5 and S6 of the left wing were shed (31st July). The tertial feathers (T7 to T9 following Jenni & Winkler [30]) started with T8 the 25th of May, followed by T9 10 days later, and finally T7 the 16th and 19th of June. The tail feathers (rectrices) were moulted in relatively short succession, starting on the 29th of May with the central pair R1 progressing outboard up to R4 with intervals of 2, 4 and 2 days, respectively. R5 was dropped 10 days after R4 and R6 9 days after R5. The time between release of the first and last flight feather was 107 days. We did not perform measurements of feather length, and therefore we have no accurate information on the time taken until feathers reached their full length, but assuming roughly 30 days to regrow each feather, the total moult process lasted about 137 days. This is similar to the moult described for wild jackdaws [31].

Wake measurements were taken at four stages during the moult. The first (stage I) was immediately after loosing P5. The bird had difficulties to glide steadily, particularly at the very low and very high speeds, resulting in relatively few usable recordings for this moult stage. The second set of wake measurements (stage II) was taken a week after stage I, before the release of P6. The next stage at which wake measurements were taken (stage III) was right after the bird dropped P9 and the last (stage IV) after loosing P10 (figure 4). For the latter two stages the recordings were obtained over two days. The bird was also flown in the wind tunnel in training sessions that were not recorded, minimizing the risk of the bird developing its skills during the experiment. In the early stages of moult the body weight of the bird decreased. At stage I the weight had reduced with 8% compared to pre-moult. At stage II weight was 6% less than pre-moult. During stage III the weight was only 1% less than pre-moult, and at stage IV the bird had returned to its original pre-moult weight.

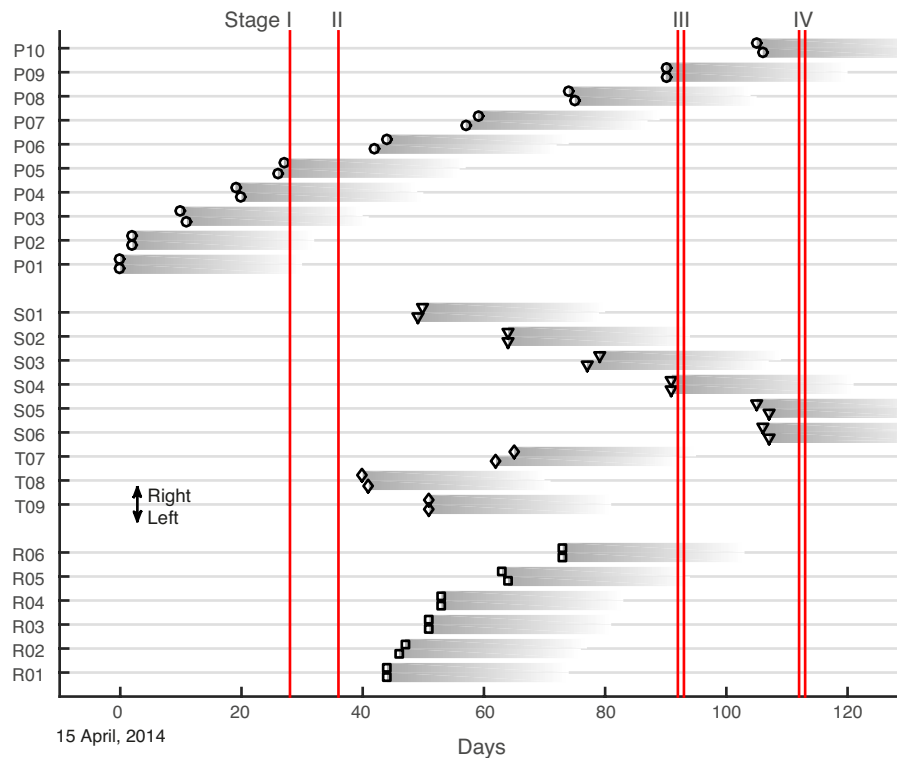


**Figure 4:** Sequence of flight feather moult. Markers indicates the release of a feather (primaries circles, secondaries triangles, tertials diamonds and rectrices squares). The bars indicate a length of 30 days, corresponding approximately with growth rate of P1 to P3 as observed in first two moult sessions. For each pair, the lower marker represents the left and the upper the right feather. The (red) vertical lines indicate the days at which PIV measurements were performed.

### 3.2. Posture

Figure 5 shows how the glide posture at different speeds changed throughout the moult. The general patterns of wing flexion and tail folding as a function of speed are similar throughout the moult period. The position of the tertials (particularly T7) was more outboard during the moult, especially in the last two stages, where the tertials cover the location of the missing inner secondaries. In stage III P9 is missing and P8 had only reached about half its final length, and it consistently overlapped with P10, which had a similar length as P8. In stage IV it is P10 that is missing and P9, still short, takes over its position.

Wingspan decreased with speed as illustrated in figure 6a. The fitted curves are quadratic polynomials with speed, with their 95% confidence bounds, which were found to best capture the variation in span ratio (Linear regression model  $\beta \sim 1 + U * U * MS$ , with span ratio  $\beta = b'_w/b_w$ , flight speed  $U$  and MS a categorical variable for moult stage,  $N = 146$ ,  $rmse = 0.031$ ,  $r^2 = 0.81$ ). Stages I and II are indistinguishable from the pre-moult. For stages III and IV the span is generally reduced compared to the pre-moult conditions. This difference is most pronounced at the lowest speeds, but interestingly, also at the highest

speeds, where the in-flight span is not trivially limited by missing outer primaries. Wing area follows a pattern very similar to the wingspan, as illustrated in figure 6b, by the linear relations between span and area ( $\zeta \sim 1 + \beta + MS$ , with area ratio  $\zeta = S'/S$ ,  $N = 144$ ,  $rmse = 0.021$ ,  $r^2 = 0.95$ ). Stage I stands out, having a 5% decreased wing area ( $p \ll 0.001$ ). For stage IV a marginal increase in wing area of 1% was found ( $p < 0.003$ ).

Only stage III was affected by tail moult, with the pair R6 still regrowing since 20 days. This is reflected by both a slightly different slope ( $-0.02$ ,  $p < 0.04$ ) and lower intercept ( $-0.20$ ,  $p < 0.02$ ) for the linear fit at lower speeds ( $< 10.5 \text{ m s}^{-1}$ ,  $\beta_t \sim 1 + U * MS$ , with tail span ratio  $\beta_t = b'_t/b_w$ ,  $N = 90$ ,  $rmse = 0.029$ ,  $r^2 = 0.82$ ), as shown in figure 7a. For all other moult stages variation in tail span is indistinguishable from pre-moult. At high speeds ( $> 10.5 \text{ m s}^{-1}$ ) tail span converged to about 7.5% of maximum wingspan ( $N = 35$ ,  $rmse = 0.010$ ) for all moult stages. For tail area the differences between moult stages were less pronounced (figure 7b).

There were no distinguishable differences between the variation in body angle at the different moult stages. Figure 8 shows the data points with quadratic fitted

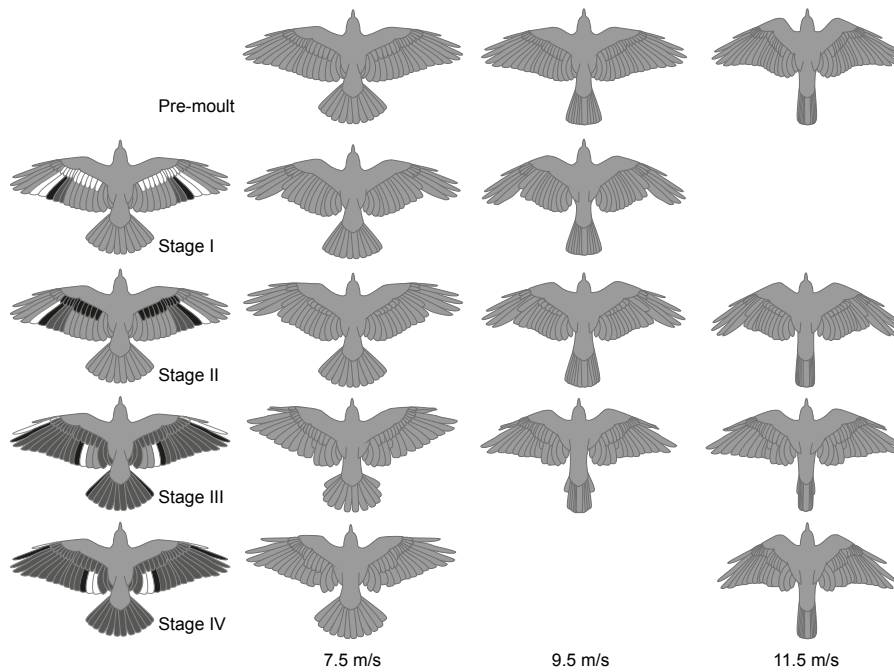


**Figure 5:** Variation in gliding posture throughout the moult. First column indicates the moult stage: white missing; black regrowing, but clearly not full length; dark grey fully replaced (as far as can be judged from the recordings). Second column corresponds to a flight speed at  $7.5 \text{ m s}^{-1}$ , third column to  $9.5 \text{ m s}^{-1}$  and fourth column to  $11.5 \text{ m s}^{-1}$ . The locations of the tips of the flight feathers (primaries, secondaries, tertials, rectrices) are to scale and determined from the reconstructed positions for the session with the lowest deviation from the average wingspan for each case. The angle of the feathers is loosely based on the position of the shoulder and wrist markers.

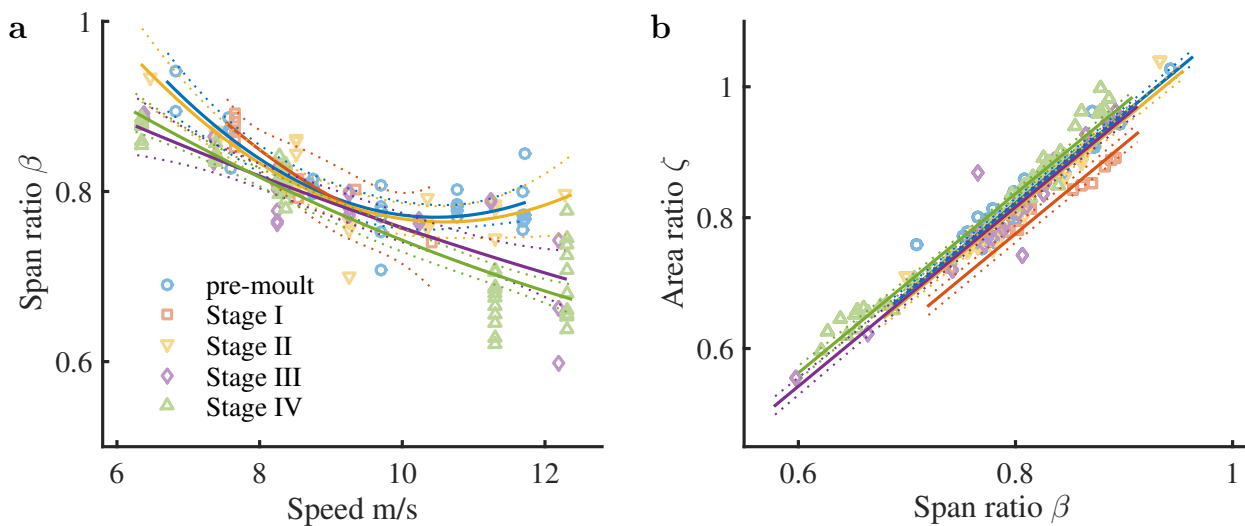


**Figure 6:** Wing posture; Symbols indicate data points, solid lines represent regression curves with corresponding 95% confidence bounds as dotted lines. (a) Variation in wingspan ratio  $\beta = b'_w/b_w$  with speed for different stages of moult. (b) Area ratio against span ratio.

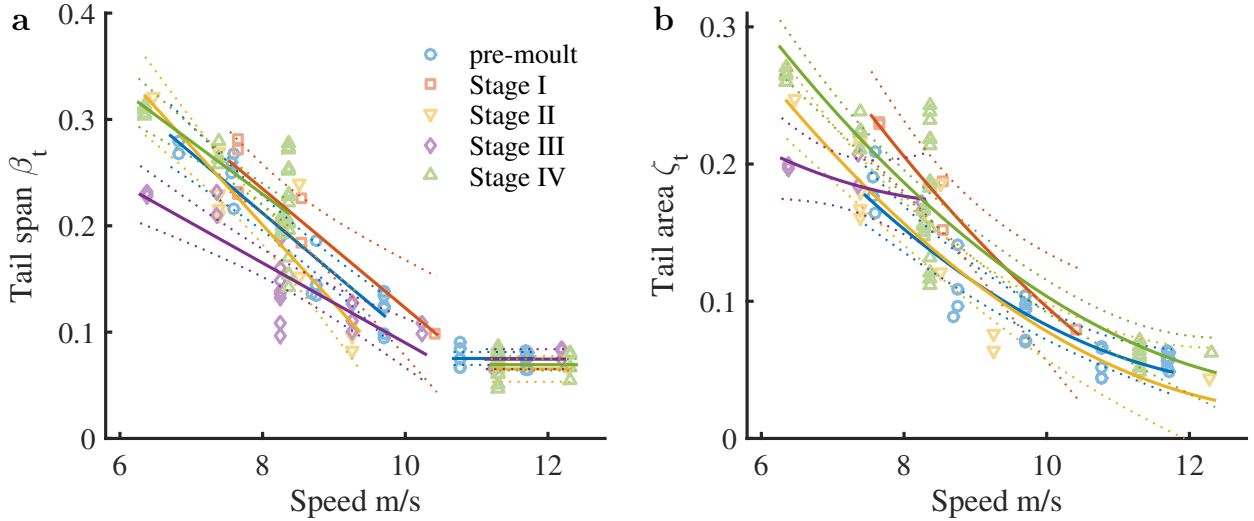


**Figure 7:** Tail posture; See legend figure 6. (a) Tail span ratio  $\beta_t = b'_t/b_w$  (relative to maximum wingspan). (b) Tail area ratio  $\zeta_t = S'_t/S_w$  (relative to maximum wing area).

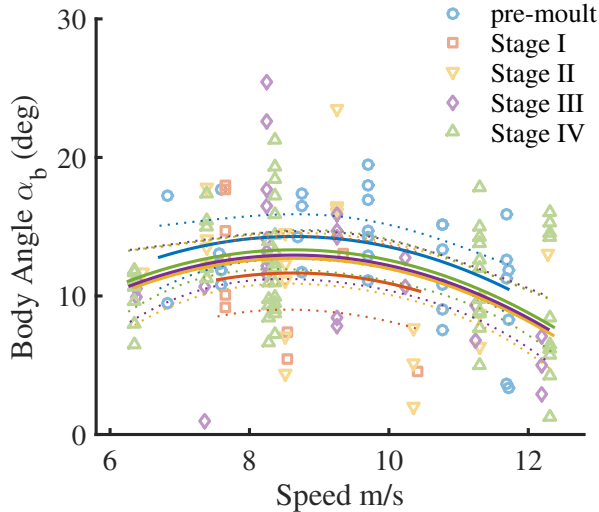


**Figure 8:** Body angle as a function of speed. See legend figure 6.

curves ( $\alpha_b \sim 1 + U * U + MS$ ,  $N = 146$ ,  $rmse = 4.18^\circ$ ,  $r^2 = 0.15$ ), with a tendency for declining body angle with increasing speed. Much of the unexplained variation should be attributed to measurement uncertainty on the positions of points (27-28).

Spanwise camber in general increased linearly with speed ( $\eta_w \sim 1 + U + MS$ ,  $N = 146$ ,  $rmse = 0.030$ ,  $r^2 = 0.62$ ) as illustrated in figure 9a. Pre-moult spanwise camber varied approximately as  $\eta_w = 0.03 + 0.012U$ . During moult stages I, II and III the spanwise camber was reduced with  $\Delta\eta_w \approx -0.05$ , which is a 30-50% decrease compared to pre-moult. At stage IV spanwise camber returned to the pre-moult level. Vertical separation of the outer primaries (P7 to P10) varied non-linearly with speed, specifically for stages

I and II. Figure 9b shows the sum of absolute vertical separation of P7 to P10 from the main wing trailing edge ( $\eta_p \sim 1 + U * U * MS$ , where  $\eta_p = \sqrt{\sum_{i=7}^{10} \eta_{p,i}^2}$ ,  $N = 146$ ,  $r.m.s.e. = 0.024$ ,  $r^2 = 0.63$ ). At medium speeds separation increased for stages I and II, while it decreased for stages III and IV. The latter reduction is not surprising, as in these stages P7-P10 are affected by moult.

Tail separation generally decreases with speed, as shown in figure 10 ( $\eta_t \sim 1 + U * MS + U * U * MS$ ,  $N = 125$ ,  $rmse = 0.012$ ,  $r^2 = 0.73$ ). At the highest speeds tail separation was negative on several occasions, corresponding to a strong local up-wash from the tail observed in corresponding wakes (e.g. figure 11h,m). At medium speeds pre-moult tail separation was somewhat larger than during moult. Stage I stands out as having a much steeper decrease of tail separation, but this seems strongly influenced by the single data point available at that speed. Otherwise, there are no discernible differences in tail separation between the moult stages.

### 3.3. Wake description

The vortex structures in the wake reflected the different stages of moult. In the pre-moult condition negative vorticity was shed more or less evenly behind the left wing (figure 11a-c). During stage I and II (row 2 and 3 in figure 11) there was a region of opposite vorticity at the location of the moult gap at P5 (figure 11d-h). On some occasions an inboard 'tip' vortex (with negative vorticity) was observed of similar strength as the true tip vortex. At stage III this discontinuity was absent (figure 11i-k). Instead, a similar, but much weaker dis-

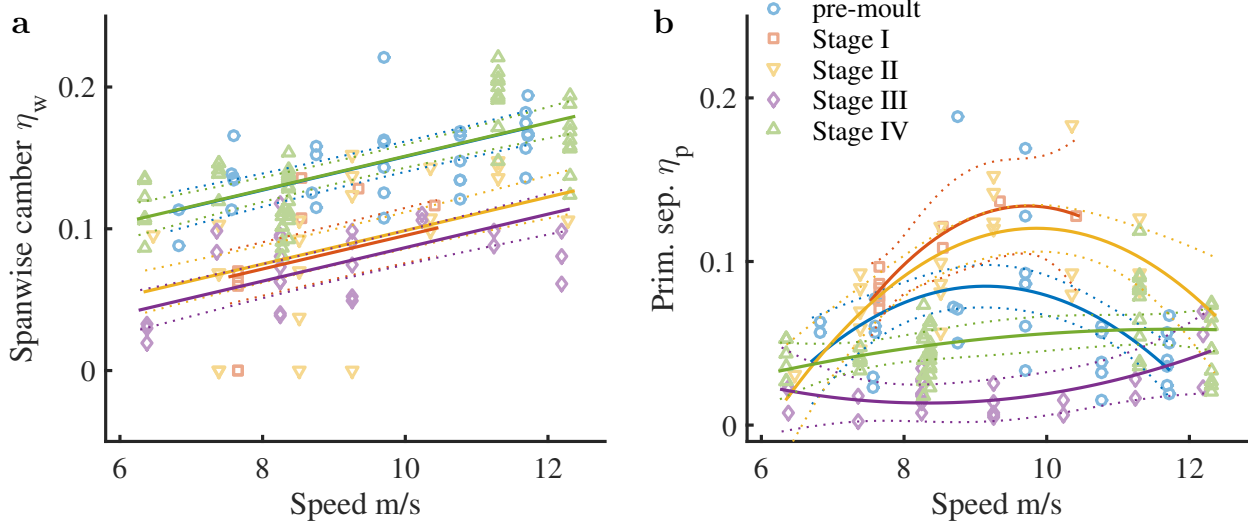


**Figure 9:** Non-planar properties of the main wing. See legend figure 6. (a) Spanwise camber as a function of speed. (b) Summed primary separation as a function of speed.

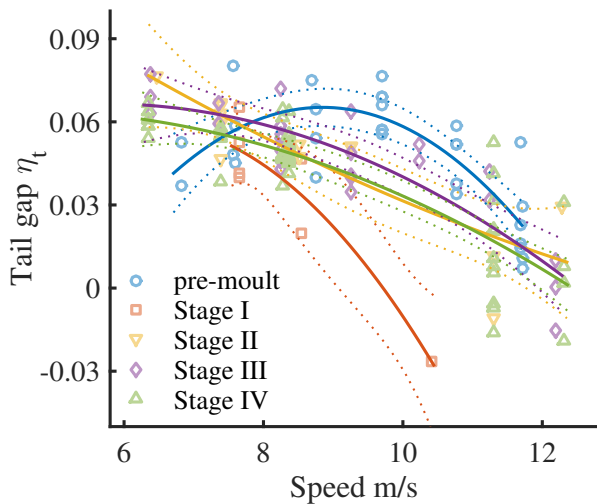


**Figure 10:** Tail separation, vertical distance between secondaries and tail trailing edges (relative to inflight wingspan). Positive values means the tail is below the main wing. See legend figure 6.

continuity was observed at the inner wing, though only at speeds below  $8 \text{ m s}^{-1}$  (figure 11i). This discontinuity corresponds to the moult gap at S4. Effects of the moult gap in the outer primaries were less obvious. In certain cases two distinct vortices were formed at the tip, and in many cases the classical tip vortex was absent, with more vorticity shed inboard of the tip. At stage IV the wakes were generally very similar to the pre-moult wakes, at least at the low speeds. At speeds above  $10 \text{ m s}^{-1}$  the wake again showed regions of opposite vorticity between the wing root and the tip (figure 11l). Consistently there were two or more tip vortices outboard of this region and also one strong vortex (with negative vorticity) some distance inboard (figure 11m). The latter corresponding to the location of the moult gap of S5/S6.

### 3.4. Components of drag

Span efficiency (based on maximum wingspan) generally decreases with flight speed, as shown in figure 12a ( $e \sim 1 + U * U * MS, 212, \text{rmse} = 0.080, r^2 = 0.65$ ). Here all moult stages differ from the pre-moult stage. Span efficiency was generally lower during moult than in the pre-moult stage. For stages II, III and IV span efficiency continues to decrease with speed at speed above  $10 \text{ m s}^{-1}$ , whereas it levels off in the pre-moult stage. Stage I shows non-linear behaviour, however, this is based on relatively few data points and should be treated with caution. Much of the variation in span efficiency is related to the in-flight wingspan. Figure 12b shows the shape specific span efficiency, where the effect of span reduction is removed. Note that these values have also been correc-

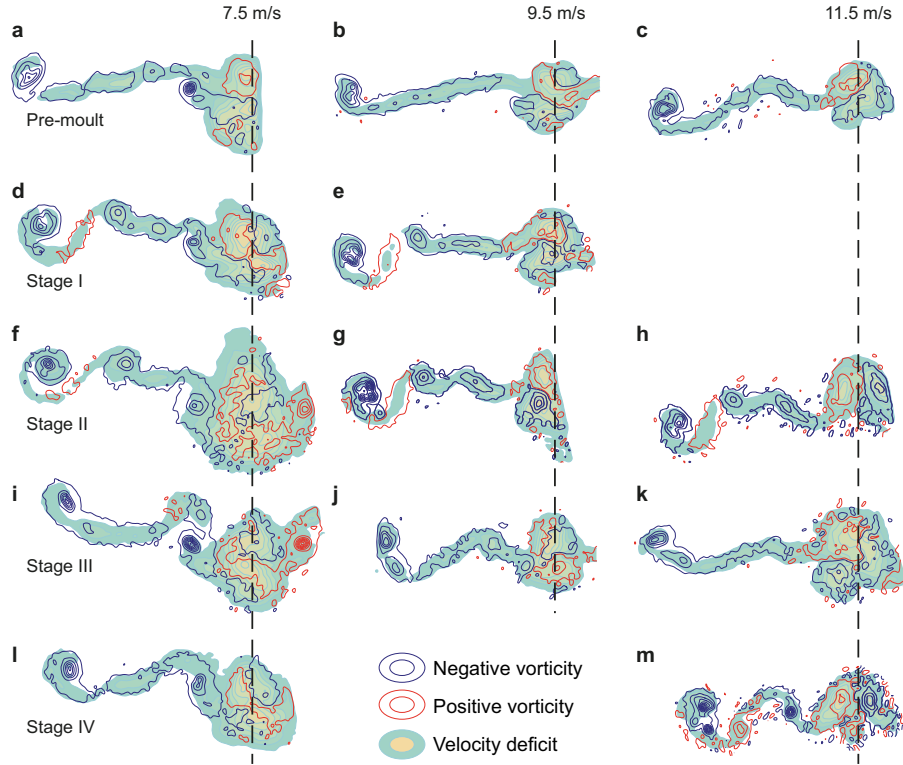
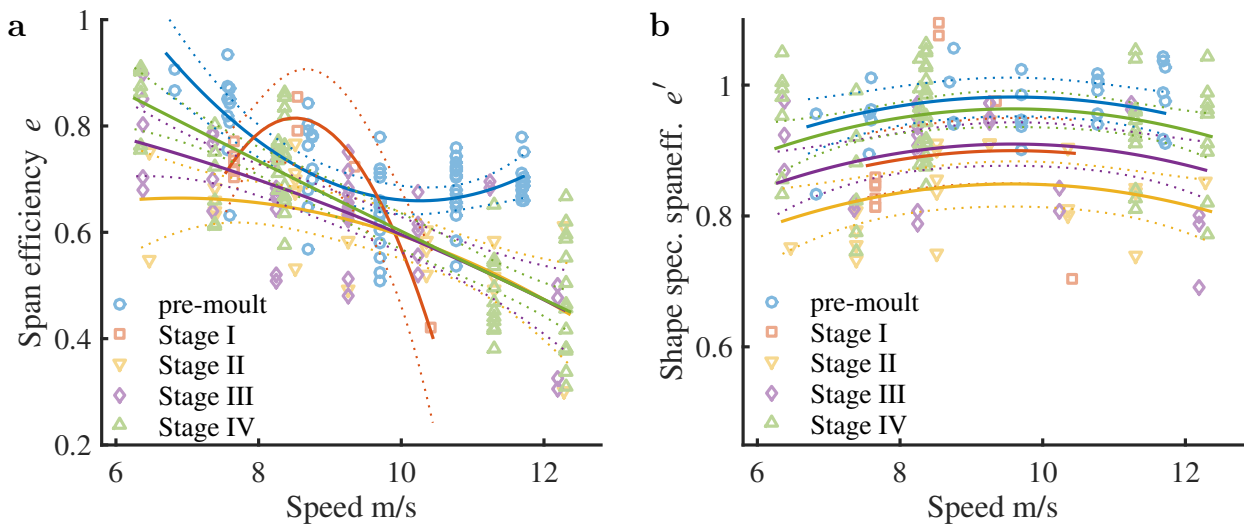


**Figure 11:** Wake structures at different speeds for different moult stages. Top row (a-c) shows wakes from the pre-moult experiments. Second row (d, e) shows wakes from moult stage I. At this stage, no usable wakes were recorded at the target speed of  $11.5 \text{ m s}^{-1}$ . Third row (f-h), fourth row (i-k) and fifth row (l, m) show stage II to IV, respectively. For stage IV no usable wakes were recorded at  $9.5 \text{ m s}^{-1}$ . These wakes correspond to the postures presented in figure 5.

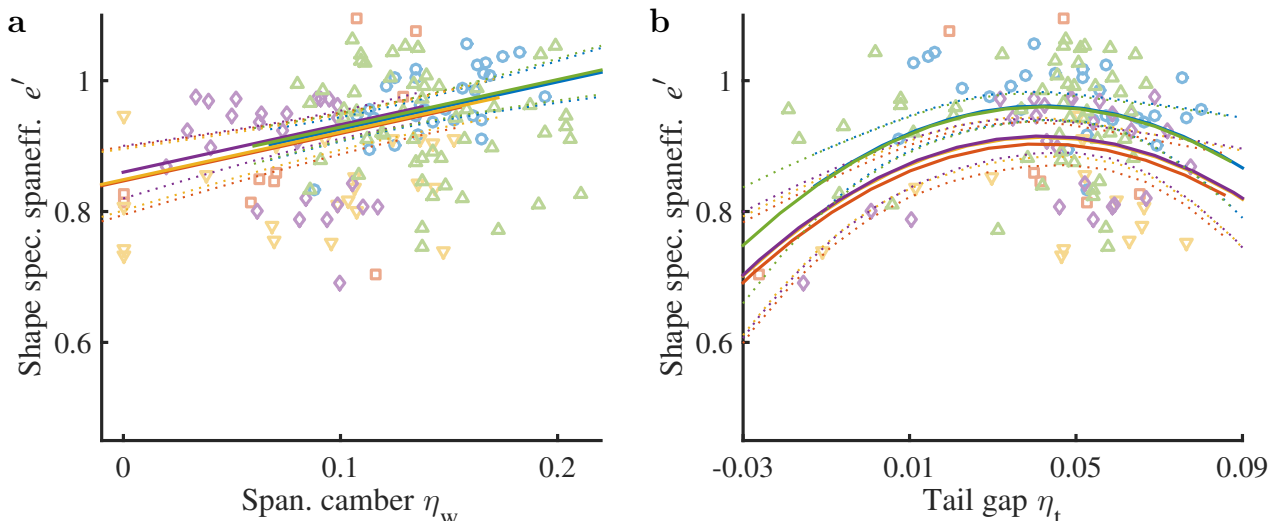
ted for wall effects. Stages I to III had reduced shape specific span efficiencies (stage I:  $-0.08 \pm 0.03(\text{s.e.})$ ,  $p < 0.001$ ; stage II:  $-0.13 \pm 0.02(\text{s.e.})$ ,  $p \ll 0.001$ , stage III:  $0.07 \pm 0.02(\text{s.e.})$ ,  $p < 0.001$ ), while at stage IV values were indistinguishable ( $p > 0.31$ ) from the pre-moult stage ( $e' \sim 1 + U * U + \text{MS}$ ,  $N = 146$ ,  $\text{rmse} = 0.077$ ,  $r^2 = 0.28$ ). It should be noted here that for stage I a strong non-linear pattern was found, but because stage I has relatively few data points and none of the other stages had significant quadratic coefficients, the quadratic term was dropped from the regression. Shape specific span efficiency depends on the load distribution across the span, and non-planar features such as spanwise camber, primary separation and the use of the tail can potentially affect this distribution. Testing for the effects of these non-planar features ( $e' \sim 1 + \eta_w + \eta_p + \eta_t^2$ ,  $N = 125$ ,  $\text{rmse} = 0.081$ ,  $r^2 = 0.23$ ), suggests that spanwise camber has a positive effect ( $0.73 \pm 0.16(\text{s.e.})$ ,  $p \ll 0.001$ ). As shown in figure 13a, this effect matches the decrease in camber across the moult stages. The regression finds a very strong effect of tail separation (figure 13b), taken as a quadratic polynomial to account for both negative and excessive positive tail lift that reduce efficiency. The fitted curves are shown together with the raw data in

figure 13b. Primary separation did not have a significant effect on efficiency ( $p > 0.48$ ).

The profile drag coefficient varied quadratically with speed, both before moult as during moult stages III and IV ( $C_{D,\text{pro}} \sim 1 + U * U * \text{MS}$ ,  $N = 208$ ,  $\text{rmse} = 0.0035$ ,  $r^2 = 0.51$ , 3 outliers removed), as shown in figure 14a. Stages I and II showed increased profile drag coefficients at medium speeds (up to a maximum increase of 48% and 51% respectively, compared to the pre-moult). Taking into account the inflight wing area, does not substantially change this pattern, as shown in figure 14b ( $C'_{D,\text{pro}} \sim 1 + U * U * \text{MS}$ ,  $N = 139$ ,  $\text{rmse} = 0.0043$ ,  $r^2 = 0.38$ , 4 outliers removed). The maximum difference at the medium speeds between stages I and II and the pre-moult now amount to an increase of 51% and 57% respectively, in  $C'_{D,\text{pro}}$  compared to pre-moult. Figure 15 shows the profile drag coefficient in relation to the lift coefficient. The fitted curves take into account primary separation and spanwise camber ( $C'_{D,\text{pro}} \sim 1 + \eta_p + \eta_w * C'_L * C'_L$ ,  $N = 140$ ,  $\text{rmse} = 0.0037$ ,  $r^2 = 0.43$ , 3 outliers removed). Spanwise camber tends to increase  $C'_{D,\text{pro}}$  at zero lift ( $0.06 \pm 0.03(\text{s.e.})$ ,  $p \approx 0.03$ ), as does primary separation ( $0.05 \pm 0.01(\text{s.e.})$ ,  $p \ll 0.001$ ). Spanwise camber also affects the linear dependency on lift coef-



**Figure 12:** Span efficiency as a function of speed. See legend figure 6. (a) Span efficiency corresponding to maximum wingspan. (b) Shape specific span efficiency, corresponding to inflight wingspan. Note that quadratic term is made independent of the moult stage, resulting in that the 'odd' behaviour of stage I in (a) is not captured by the regression.



**Figure 13:** Regression curves for shape specific span efficiency as functions of (a) spanwise camber and (b) tail separation. For each curve the remaining predictors ( $\eta_p$  and  $\eta_t$  for a, and  $\eta_w$  and  $\eta_t$  for b) are taken as their mean within each moult group.

ficient ( $p < 0.001$ ), increasing the minimum drag lift coefficient and lowering the corresponding minimum drag.

The body drag coefficient varies strongly with flight speed, where the moult stages only strongly differ from pre-moult at the lowest speeds ( $C_{D,\text{par}} \sim 1 + U * U * \text{MS}$ ,  $N = 211$ ,  $\text{rmse} = 0.078$ ,  $r^2 = 0.80$ , 1 outlier removed), as shown in figure 16a. Interestingly, stage III was more similar to pre-moult than all other stages. At the highest speeds, where body drag matters the most and the bird will be in its "cleanest" configuration,  $C_{D,\text{par}}$  averages around 0.22 for pre-moult and moult stage IV (at  $12 \text{ m s}^{-1}$ ). For the other moult stages  $C_{D,\text{par}}$  was a little higher (0.27 for II and 0.28 for III), but this difference was statistically indistinguishable among the residual variation. Because the tail wake is included in the body drag measurement, there is a strong relation between tail span and body drag coefficient ( $C_{D,\text{b}} \sim 1 + \beta_t * \beta_t + \text{MS}$ ,  $N = 124$ ,  $\text{rmse} = 0.087$ ,  $r^2 = 0.77$ , 1 outlier removed), as shown in figure 16b. Only stage II and III show a distinguishable difference with the pre-moult condition, but overall the differences appear to be small.

#### 4. Discussion

We measured how moult affected the posture and drag components in a gliding jackdaw. During moult stage I, after shedding the first 5 primary pairs, the wing area for a given wingspan was reduced with 5% due to missing feathers. At this stage the weight of the bird was also reduced by 8%, even though the bird was fed *ad libitum*. This means that the reduced wing area had only a small effect on the wing loading, i.e. the weight reduction compensates for the loss of wing area. In stage II, with P3 mostly grown back, the wing area was not notably different from the other stages, while the weight was still 6% reduced, suggesting an even lower wing loading. In the subsequent moult stages the in-flight wing area was not substantially reduced compared to pre-moult, and the weight returned to pre-moult levels. A similar pattern of weight loss during moult was found in hummingbirds by Chai [15], which likewise appeared to compensate for the reduced wing area by losing weight, diminishing the effect of moult on their flight metabolism. That we find this also for a jackdaw suggests weight loss may be a common strategy during moult.

Our qualitative interpretation of the glide posture suggests that during moult the bird adjusts its wing shape to compensate for missing feathers. The elbow was moved outboard, resulting in a gap between the

body and the tertials, but allowing adjacent feathers to partially cover the moult gaps. This was most apparent at stage III and IV when the inner secondaries were moulted. But also in stage I and II, where P4 and P5 were missing, the more inboard feathers seemed to partially cover the gap (figure 5). That it is the inner wing that moves outwards, rather than the outer wing moving inwards, is corroborated by the fact that stages I and II do not seem to affect the inflight wingspan. Only when the outer primaries are moulting, was the wingspan reduced.

Even though wingspan was not affected in stages I and II, span efficiency was reduced by about 15%. This effect was correlated with a strong reduction in spanwise camber at these moult stages. Jackdaws typically glide with a spanwise camber where the wingtips are pressed down (anhedral). Anhedral is normally associated with roll stability [32], assumed to come at the cost of increased induced drag due to the inevitable span reduction. In normal conditions feathers are prevented from bending up under aerodynamic loads by proximal feathers partially covering it. With P4 and P5 missing, the outer primaries are free to collectively bend up, reducing the typical spanwise camber. The correlation between spanwise camber and span efficiency could imply that the spanwise camber plays an essential role for efficient lift production.

In most literature the vertical separation of the outer primaries is attributed to the function of improving span efficiency. Tucker [22] clipped the outer primaries of a Harris' hawk and studied the effect of this manipulation on the total drag. A strong reduction (44%) in span efficiency was inferred, assuming the profile drag and body drag coefficients were unaffected. In stage III the jackdaw was moulting the outer primaries, a situation that bears resemblance to the Harris' hawk with clipped primaries. This resulted in a reduced primary separation, and a reduction in span efficiency of 7% compared to pre-moult. However, this decrease also coincides with a reduction in spanwise camber, which seemed to explain the difference in span efficiency for stages I and II. In many of the cases with strong spanwise camber, the vertical shape of the wing resembled a circular arc segment, which has a theoretical maximum span efficiency of  $e' = 1 + \eta_w^2$  [20]. When inspecting figure 13a, the first thing to notice is that span efficiency is generally below 1 and, second, the observed range of spanwise camber would only account for a variation of about 4% in efficiency. This suggests the wing is never 'optimally' loaded and the variation in  $\eta_w$  coincides with two distinct mechanisms for  $e'$  to

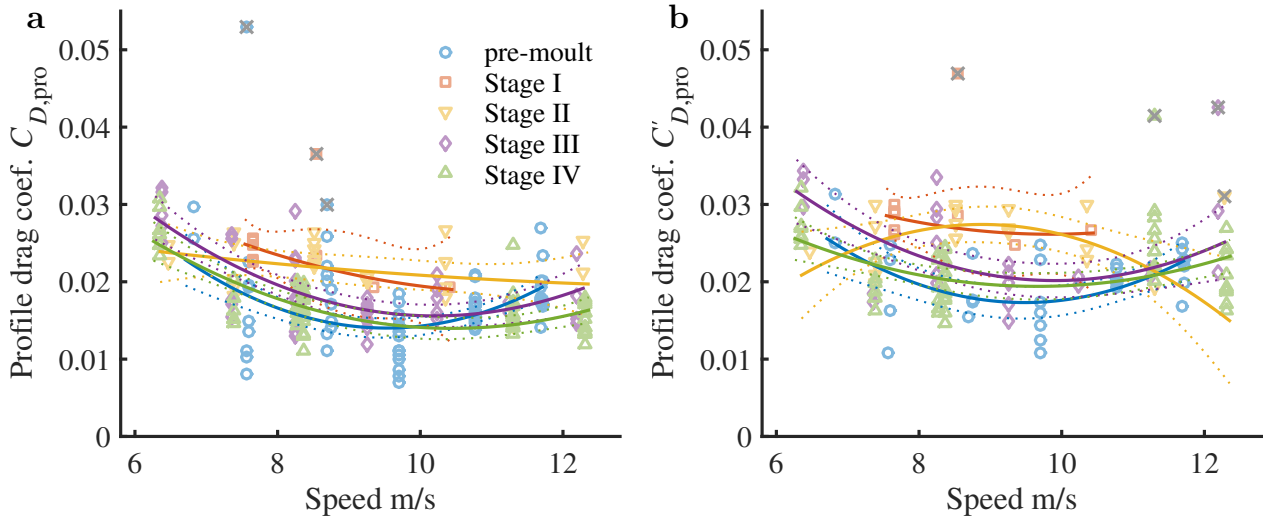


**Figure 14:** Wing profile drag coefficient as a function of speed. See legend figure 6. (a) Profile drag coefficient corresponding to maximum wing area. (b) Shape specific profile drag coefficient, corresponding to inflight wing area.

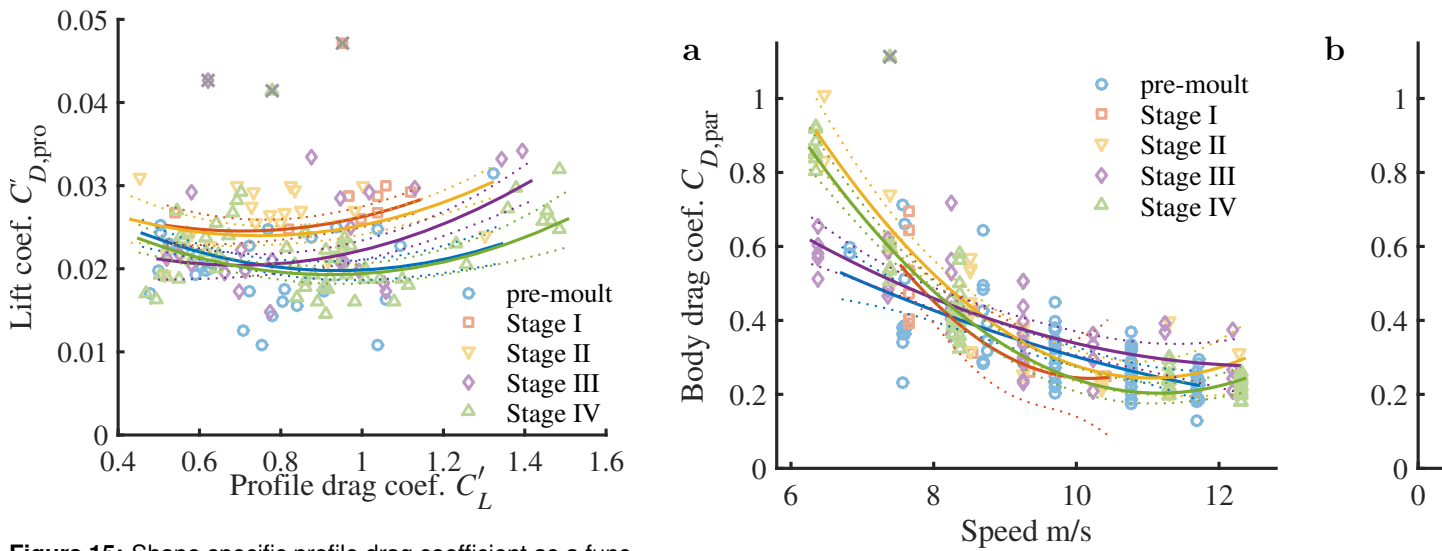


**Figure 15:** Shape specific profile drag coefficient as a function of shape specific lift coefficient. Regression is based on lift coefficient  $C'_L$ , spanwise camber  $\eta_w$  and primary separation  $\eta_p$  (instead of moult stage). For the displayed curves  $\eta_w$  and  $\eta_p$  were taken as the mean per moult stage.

**Figure 16:** Body drag coefficient based on body frontal area  $S_b$ . See legend figure 6. (a) As a function of speed. (b) As a function of tail span, illustrating the effect of tail profile drag.

decrease: In stage I and II a gap between the arm and hand wing caused a strong discontinuity in the lift distribution, deteriorating  $e'$ , whereas in stage III the loss of primary separation caused a reduction in  $e'$ , i.e. a less efficient shape of the wing-tip.

The profile drag coefficient,  $C'_{D,pro}$ , substantially increased for moult stages I and II, with up to 50% near the minimum drag flight speed. Here, primary separation seems to play an important role. An explanation for this may be due to increased friction at low Reynolds numbers. For a laminar flow over a flat plate the friction coefficient is  $C_{D,f} \propto Re_c^{-1/2}$ , where  $Re_c = cU/\nu$ ,  $c$  being the chord length of the plate, and  $\nu$  the kinematic viscosity of air. Splitting a surface in  $n$  separated elements causes the Reynolds number of each section to be lower, giving each element a higher drag coefficient. If all segments are of equal length, this results in a combined friction coefficient being  $\sqrt{n}$  times that of the original flat plate. For the 3 outer primaries of the jackdaw wing, this may amount to a localized 70% increase in friction coefficient. Interestingly  $C'_{D,pro}$  also appears to depend on spanwise camber, decreasing the minimum drag and shifting it to higher lift coefficients. As spanwise camber is reduced during stages I and II, their polar curves are shifted up and to the left in figure 15. At stage III spanwise camber was similarly reduced, but also primary separation had decreased to a minimum, thereby lowering the entire curve compared to stages I and II. At  $11 \text{ m s}^{-1}$  by flexing the wings, reducing the wing area by about 25%, the lift coefficient is raised from 0.44 to 0.58. With a spanwise camber of  $\eta_w = 0.1$  this reduces the profile drag by 0.0015, an improvement of 7%. Together with the decrease in area, this amounts to a reduction in profile drag of 30%. With no spanwise camber,  $\eta_w = 0$ , the same difference in  $C'_L$  would instead increase  $C_{D,pro}$  with 1%, so that the span reduction only reduces profile drag by 24%.

The effects of moult on the body drag appear to be minor. Body drag coefficient is strongly related with tail span, indicating the important role of tail profile drag. For moult stage III the maximum tail span was reduced by the moult of the rectrices, so it is expected that body drag coefficient is larger for any given tail span, as found in figure 16b. For moult stage II and IV the body drag coefficient approaches unity at the lowest speeds. As seen in figure 16b, these extreme values deviate from the general relation with tail span, suggesting they are not due to tail profile drag. Instead, these high measures for body drag are likely associated with lowering of the legs, which act as air

brakes. We observed the lowering of the legs at low speeds, but our camera setup did not allow for quantification of leg extension. At these low speeds dynamic pressure is very low, so that the bird can use these brakes to control the drag with great precision. Additionally, with the extension of the legs the bird can adjust both the location of the resultant aerodynamic force and the location of the centre of gravity, helping it to find the correct balance (trim condition). Attributing this deviation from the general relation with tail span to leg extension would suggest that the bird uses its legs more frequently across the speed range during tail moult (stage III).

#### 4.1. Concluding remarks

From our measurements of aerodynamic performance during the moult of a jackdaw we can conclude that the bird experienced substantial reductions in glide efficiency. The negative effects are partially mitigated by adjustments of wing posture to minimize gaps in the wing, and by mass loss to reduce wing loading. This is a study of only a single jackdaw, during a single moult, so we should be careful when generalizing our results. However, our findings are in line with other studies [31, 14, 15, 2]. The data we present are on gliding flight, but we expect that moult will affect flapping flight in similar ways. However, the quantitative consequences for powered flight should be investigated further, as for example the wing deformation of the outer wing observed in stages I and II may have pronounced consequences for the efficiency of thrust production.

We found that the impact on aerodynamic performance differs for different moult stages, where the moult of the inner primaries appears to have the most substantial impact, increasing both induced drag and profile drag. This implies that this particular moult strategy does not aim to spread out the aerodynamic cost of moult equally over the moult period. It is possible that suffering a relatively high aerodynamic cost early during the moult serves to minimize the additional wear to freshly moulted feathers during later stages of moult. Other bird species may have different tolerances regarding the reduction of aerodynamic performance, which would explain why some have evolved alternative moulting patterns [6, 7].

In addition to the aerodynamic costs of moult a bird also needs to cover the increased costs of thermoregulation and growth of new feathers [33, 34]. Together, the elevated costs during moult may explain why moult rarely coincides with other demanding processes in the annual cycle, such as feeding young and migra-

tion [35]. Wild jackdaws breed in the spring and after breeding they initiate moult.

The moult strategies employed by birds could also inspire solutions for alleviating wing damage in man-made aircraft. Particularly micro aerial vehicles (MAVs) have potential to benefit from our results, for example by developing morphing wings.

## List of symbols

$b$  Span (m);  $b_w$  wing span;  $b'_w$  in-flight wing span;  $b'_t$  in-flight tail span

$C_{<, >}$  Force coefficient (-);  $C_D$  drag coefficient;  $C_L$  lift coefficient;

$D$  Drag (N);  $D_{ind}$  induced drag;  $D_{pro}$  wing profile drag;  $D_{par}$  body drag

$e$  Span efficiency (-);  $e'$  in-flight span efficiency

$L$  Lift (N)

$q$  Dynamic pressure (Pa);  $q = \frac{1}{2}\rho U_\infty^2$

$Re$  Reynolds number  $Re = U\ell/\nu$  with  $U$  the airspeed,  $\ell$  a characteristic length and  $\nu$  the kinematic viscosity of air.

$S$  Area (m<sup>2</sup>);  $S_w$  wing area;  $S_b$  body frontal area

$\mathbf{u}$  Velocity field vector  $\mathbf{u} = (u, v, w)^T$ ;  $\bar{\mathbf{u}}$  time averaged velocity field;  $\mathbf{u}'$  root-mean-square of temporal fluctuations

$u, v, w$  Wake velocity field components (m s<sup>-1</sup>);  $u$  downstream;  $v$  spanwise;  $w$  'vertically' up

$U_\infty$  Free stream velocity (m s<sup>-1</sup>)

$W$  Weight (N)

$x, y, z$  Coordinate system, with  $x$  pointing downstream,  $y$  in spanwise direction and  $z$  'vertically' up

$\beta$  Span ratio (-); in-flight span to reference span  $b'/b$

$\gamma$  Glide angle (°)

$\zeta$  Area ratio (-); in-flight area ratio to reference area  $S'/S$

$\eta$  Height normalized by in-flight wingspan  $\eta = z/b'$ ;  $\eta_w$  spanwise camber;  $\eta_p$  primary separation;  $\eta_t$  vertical tail separation

$\sigma$  Wall correction (-); numerically obtained wall correction factor for induced drag

$\psi$  Stream function (m<sup>2</sup> s<sup>-1</sup>)

$\omega$  Streamwise vorticity (s<sup>-1</sup>);  $\bar{\omega}$  vorticity from the averaged velocity field

**Acknowledgements** We thank Johan Nilsson for providing us with the jackdaw. We are also grateful to the other members of the Animal Flight Lab for their occasional assistance during the experiments and with taking care of the jackdaw.

**Competing interests** No competing interests

**Authors' contributions** M.K. and A.H. conceived the study; M.K. trained the bird and carried out the experiments, analysed the data and drafted the manuscript.

**Funding** The research received funding from the Knut and Alice Wallenberg foundation to A.H., from the Swedish Research Council to A.H. (621-2009-4965/621-2012-3585), from an infrastructure grant from Lund University to A.H., and from the Royal Physiographic Society in Lund to M.K.. This work received support from the Centre for Animal Movement Research (CANMove) financed by a Linnaeus grant (349-2007-8690) from the Swedish Research Council and Lund University.

**Ethics statement** This study involved experiments on animal subjects, which were carried out under permission M 33-13 from the Malmö-Lund animal ethics committee.

**Data availability** The compiled dataset with force data and posture measures is uploaded as supplementary material (ESM 1). Raw data can be made available on request.

## References

- [1] King, J. R. 1974 Seasonal allocation of time and energy resources in birds. In *Avian energ.* (ed. R. A. Paynter), pp. 1–85. Cambridge, Massachusetts: Nuttall Ornithological Club.
- [2] Hedenström, A. & Sunada, S. 1999 On the aerodynamics of moult gaps in birds. *J. Exp. Biol.*, **202**(1), 67–76.
- [3] Haukioja, E. 1971 Flightlessness in some moulting passerines in Northern Europe. *Ornis Fenn.*, **48**, 101–116.
- [4] Sjöberg, K. 1988 The flightless period of free-living male Teal *Anas crecca* in northern Sweden. *Ibis (Lond. 1859)*, **130**, 164–171.
- [5] De Roo, A. 1966 Age-characteristics in adult and subadult swifts, *Apus a. apus* (L.), based on interrupted and delayed wing-moult. *Gerfaut*, **56**(2), 113–134.
- [6] Edelstam, C. 1984 Patterns of moult in large birds of prey. *Ann. Zool. Fennici*, **21**(3), 271–276.
- [7] Zuberogoitia, I., Gil, J. A., Martínez, J. E., Erni, B., Aniz, B. & López-López, P. 2015 The flight feather moult pattern of the bearded vulture (*Gypaetus barbatus*). *J. Ornithol.* (doi: 10.1007/s10336-015-1269-3)
- [8] Prince, P. a., Rodwell, S., Jones, M. & Rothery, P. 1995 Moult in Black-browed and Grey-headed Albatrosses *Diomedea melanophris* and *D. chrysostoma*. *Ibis (Lond. 1859)*, **135**, 121–131. (doi:10.1111/j.1474-919X.1993.tb02823.x)
- [9] Langston, N. E. & Rohwer, S. 1996 Implications Life History in Albatrosses: Tradeoffs for Big Birds. *Oikos*, **76**(3), 498–510.
- [10] Boano, G., Pellegrino, I. & Cucco, M. 2015 Moult and Morphometrics of the Pallid Swift *Apus pallidus* in Northwestern Italy. *Ardeola*, **62**(1), 35–48. (doi:10.13157/arla.62.1.2015.35)
- [11] Jukema, J., van de Wetering, H. & Klaassen, R. H. G. 2015 Primary moult in non-breeding second-calendar-year Swifts *Apus apus* during summer in Europe. *Ringing Migr.*, **30**(1), 1–6. (doi:10.1080/03078698.2015.1059632)
- [12] Hall, K. S. S. & Fransson, T. 2000 Lesser Whitethroats under time-constraint moult more rapidly and grow shorter wing feathers. *J. Avian Biol.*, **31**, 583–587. (doi:10.1034/j.1600-048X.2000.310419.x)
- [13] Svensson, E. & Hedenström, A. 1999 A phylogenetic analysis of the evolution of moult strategies in Western Palearctic warblers (*Aves: Sylviidae*). *Biol. J. Linn. Soc.*, **67**(2), 263–276. (doi:10.1006/bijl.1998.0302)
- [14] Tucker, V. A. 1991 The effect of molting on the gliding performance of a Harris' Hawk (*Parabuteo unicinctus*). *Auk*, **108**(January), 108–113.
- [15] Chai, P. 1997 Hummingbird hovering energetics during moult of primary flight feathers. *J. Exp. Biol.*, **200**, 1527–1536.
- [16] Lind, J. 2001 Escape flight in moulting Tree Sparrows (*Passer montanus*). *Funct. Ecol.*, **15**(1), 29–35. (doi:10.1046/j.1365-2435.2001.00497.x)
- [17] Williams, E. V. & Swaddle, J. P. 2003 Moult, flight performance and wingbeat kinematics during take-off in European starlings *Sturnus vulgaris*. *J. Avian Biol.*, **34**(4), 371–378. (doi:10.1111/j.0908-8857.2003.02964.x)

- [18] Johansson, L. C. & Hedenström, A. 2009 The vortex wake of blackcaps (*Sylvia atricapilla* L.) measured using high-speed digital particle image velocimetry (DPIV). *J. Exp. Biol.*, **212**(Pt 20), 3365–3376. (doi:10.1242/jeb.034454)
- [19] Tucker, V. A. 1987 Gliding birds: the effect of variable wing span. *J. Exp. Biol.*, **133**(1), 33–58.
- [20] Cone, C. D. 1962 NASA TR R-139 The Theory of Induced Lift and Minimum Induced Drag of Nonplanar Lifting Systems. Tech. rep., National Aeronautics and Space Administration.
- [21] Tucker, V. A. 1993 Gliding birds: reduction of induced drag by wing tip slots between the primary feathers. *J. Exp. Biol.*, **180**(1), 285–310.
- [22] Tucker, V. A. 1995 Drag reduction by wing tip slots in a gliding Harris' hawk, *Parabuteo unicinctus*. *J. Exp. Biol.*, **198**(Pt 3), 775–81.
- [23] Thomas, A. L. R. 1996 Why do birds have tails? The tail as a drag reducing flap, and trim control. *J. Theor. Biol.*, **183**, 247–253.
- [24] Pennycuik, C. J., Alerstam, T. & Hedenström, A. 1997 A new low-turbulence wind tunnel for bird flight experiments at Lund University, Sweden. *J. Exp. Biol.*, **200**(Pt 10), 1441–9.
- [25] KleinHeerenbrink, M., Warfvinge, K. & Hedenström, A. 2016 Wake analysis of aerodynamic components for the glide envelope of a jackdaw (*Corvus monedula*). *J. Exp. Biol.*, **219**(10), 1572–1581. (doi:10.1242/jeb.132480)
- [26] Pennycuik, C. J. 2008 *Modelling the flying bird*. Amsterdam, The Netherlands: Elsevier.
- [27] Hedenström, A. & Rosén, M. 2003 Body frontal area in passerine birds. *J. Avian Biol.*, **34**(2), 159–162. (doi:10.1034/j.1600-048X.2003.03145.x)
- [28] van Dam, C. P., Nikfetrat, K. & Vijgen, P. M. H. W. 1993 Lift and drag calculations for wings and tails: Techniques and applications. In *Fluid dyn. biol.* (eds A. Y. Cheer & C. P. Van Dam), pp. 463–472. American Mathematical Society. (doi: <http://dx.doi.org/10.1090/conm/141>)
- [29] Barlow, J. B., Rae, W. H. & Pope, A. 1999 *Low-speed wind tunnel testing*. Wiley, 3rd edn.
- [30] Jenni, L. & Winkler, R. 1994 *Moult and Ageing of European Passerines*. London: Academic Press, first edit edn.
- [31] Ginn, H. B. & Melville, D. 1983 *Moult in birds (BTO Guide 19)*. Tring: British Trust for Ornithology.
- [32] Thomas, A. L. R. & Taylor, G. K. 2001 Animal flight dynamics I. Stability in gliding flight. *J. Theor. Biol.*, **212**(3), 399–424. (doi:10.1006/jtbi.2001.2387)
- [33] Lindström, Å., Visser, G. H. & Daan, S. 1993 The energetic cost of feather synthesis to basal metabolic rate is proportional. *Physiol. Zool.*, **66**(4), 490–510.
- [34] Lustick, S. 1970 Energy requirements of molt in cowbirds. *Auk*, **87**(4), 742–746.
- [35] Barta, Z., McNamara, J. M., Houston, A. I., Weber, T. P., Hedenström, A. & Feró, O. 2008 Optimal moult strategies in migratory birds. *Philos. Trans. R. Soc. B Biol. Sci.*, **363**(1490), 211–229. (doi:10.1098/rstb.2007.2136)